Available online at www.sciencedirect.com

SCIENCE DIRECT®

International Journal of Approximate Reasoning
41 (2006) 343–368

INTERNATIONAL JOURNAL OF APPROXIMATE REASONING

www.elsevier.com/locate/ijar

Fuzzy-hybrid modelling of an Ackerman steered electric vehicle

J.T. Economou *, R.E. Colyer

Department of Aerospace, Power and Sensors, Cranfield University, RMCS Shrivenham, Swindon SN6 8LA, England, UK

Received 1 April 2004; received in revised form 1 November 2004; accepted 1 August 2005
Available online 21 November 2005

Abstract

Physical system modelling with known parameters together with 2-D or high order look-up tables (obtained from experimental data), have been the preferred method for simulating electric vehicles. The non-linear phenomena which are present at the vehicle tyre patch and ground interface have resulted in a quantitative understanding of this phenomena. However, nowadays, there is a requirement for a deeper understanding of the vehicle sub-models which previously used look-up tables. In this paper the hybrid modelling methodology used for electric vehicle systems offers a two-stage advantage: firstly, the vehicle model retains a comprehensive analytical formulation and secondly, the 'fuzzy' element offers, in addition to the quantitative results, a qualitative understanding of specific vehicle sub-models. In the literature several hybrid topologies are reported, sequential, auxiliary, and embedded.

In this paper, the hybrid model topology selected is auxiliary and within the same hybrid model, the first paradigm used is the vehicle dynamics together with the actuator/gearbox system. The second paradigm is the non-linear fuzzy tyre model for each wheel. In particular, conventional physical system dynamic modelling has been combined with the fuzzy logic type-II or type-III methodology. The resulting hybrid-fuzzy tyre models were estimated for a-priori number of rules from experimental data. The physical system modelling required the available vehicle parameters such as the overall mass, wheel radius and chassis dimensions. The suggested synergetic fusion of the two methods, (hybrid-fuzzy), allowed the vehicle planar trajectories to be obtained prior to the hardware development of the entire vehicle. The strength of this methodology is that it requires localised system experimental data rather than global system data. The disadvantage in obtaining global experimental data is the requirement for comprehensive testing of a vehicle prototype which is both time consuming

* Corresponding author. Tel.: +44 (0)1793 785206; fax: +44 (0)1793 785902.
E-mail addresses: J.T.Economou@cranfield.ac.uk (J.T. Economou), r.e.colyer@cranfield.ac.uk (R.E. Colyer).

0888-613X/$ - see front matter
doi:10.1016/j.ijar.2005.08.002

process and requires extensive resources. In this paper the authors have proposed the use of existing experimental rigs which are available from the leading automotive manufacturers. Hence, for the 'hybrid' modelling, localised data sets were used. In particular, wheel-tyre experimental data were obtained from the University Tyre Rig experimental facilities. Tyre forces acting on the tyre patch are mainly responsible for the overall electric vehicle motion. In addition, tyre measurement rigs are a well known method for obtaining localised data thus allowing the effective simulation of more detailed mathematical models. These include, firstly, physical system modelling (conventional vehicle dynamics), secondly, fuzzy type II or III modelling (for the tyre characteristics), and thirdly, electric drive modelling within the context of electric vehicles. The proposed hybrid model synthesis has resulted in simulation results which are similar to piece-wise 'look-up' table solutions. In addition, the strength of the 'hybrid' synthesis is that the analyst has a set of rules which clearly show the reasoning behind the complex development of the vehicle tyre forces. This is due to the inherent transparency of the type II and type III methodologies. Finally, the authors discussed the reasons for selecting a type-III framework. The paper concludes with a plethora of simulation results.

Keywords: Hybrid model synthesis; Type-II and type-III fuzzy systems; Parameter estimation; Electric drives

1. Introduction

In this paper a single electric actuator consisting of a permanent magnet direct current (PMDC) geared motor is used to drive the rear wheels of a small-scale vehicle.

Currently, conventional methods concentrate mainly in the analysis of the dynamics with the drive actuators excluded. However, here the actuator forms an integral part of the overall model.

To complement the conventional modelling approach fuzzy logic was also used to model the tyre non-linear cornering forces which are generated during steering. Fuzzy logic belongs to the class of ''intelligent'' methods [1,2] which are based on ''knowledge based'' methodologies. Conventional modelling methods, when applied to practical problems, have demonstrated the difficulty of representing accurately a complex process by a single mathematical model over a wide range of input demands. Recently, there has been increasing interest in the application of intelligent methods in solving such practical problems.

In particular, ''intelligent modelling'' forms part of the ''hybrid modelling'' (HM) approach which fuses conventional mathematical modelling techniques and ''intelligent'' techniques such as fuzzy logic [3], neural networks [4,5], genetic algorithms [6] and/or heuristics. The HM representation can provide a high fidelity vehicle model, for example, without the computational cost of increased dimensionality when compared with models derived simply using strictly intelligent based methods. In effect, the HM approach, as shown in this paper, complements the conventional mathematical modelling based methods by means of physical modelling and type-II and type-III fuzzy systems.

It is well accepted that the tyre, although being a small proportion of a vehicle, is an important and complex non-linear component. In this paper, a hybrid mathematical modelling approach is presented which complements the conventional approaches reported in the literature. The tyre is modelled using both type-II and type-III fuzzy systems, which have been estimated from experimental tyre data, using a nonlinear least-squares multi-

Nomenclature

u	center of gravity (CG) longitudinal velocity
v	CG lateral velocity
r	CG yaw rate
α_{f}	front tyre slip angle
α_{r}	rear tyre slip angle
u_{f}	front longitudinal component of the sideslip velocity
u_{r}	rear longitudinal component of the sideslip velocity
v_{f}	front lateral component of the sideslip velocity
v_{r}	rear lateral component of the sideslip velocity
δ	mean Ackerman steering demand
β	CG sideslip angle
β_{f}	front track sideslip angle
β_{r}	rear track sideslip angle
l_{f}	CG to front track distance
l_{r}	CG to rear track distance
R	wheel radius
m	vehicle mass
n_{g}	step-down gearbox
R_{a}	motor armature resistance
K_{T}	motor torque constant
V_{a}	PMDC armature voltage
ω_{m}	motor angular velocity
T_{m}	motor supplied torque
$F_{\mathrm{r}}^{[\mathrm{f},\mathrm{r}]}$	vehicle rolling resistance
F_x	total longitudinal force
F_x^{f}	front tyre induced force
K_{r}	rolling coefficient
f	front wheel
r	rear wheel
$F_y^{[\mathrm{f},\mathrm{r}]}$	lateral wheel force
$\alpha_{[\mathrm{f},\mathrm{r}]}$	tyre slip angle
$\frac{\partial F_y}{\partial \alpha}$	tyre cornering stiffness
$C_{\alpha_{[\mathrm{f},\mathrm{r}]}}$	linearised tyre cornering stiffness
q	fuzzy rule number
j	fuzzy variable index
c_q	membership function centre
d_q	membership function spread
A_q^j	qth fuzzy set for the jth fuzzy input variable
μ_{A_q}	membership function
λ_q	multi-variable fusion for the qth rule
γ	Sugeno fuzzy offset

objective setting. The fused type-II, and type-III fuzzy tyre models retain their initial non-linear characteristics. The local models also retain an explicit mathematical hybrid formulation due to:

(a) the physical system modelling,
(b) the type-II and type-III explicit mathematical fuzzy consequent descriptions.

Furthermore, the analysis using fuzzy type-II and type-III models of the entire tyre non-linear envelope enable the vehicle to be 'tested' under rapid and aggressive steering demands and the vehicle has been simulated for a multi-frequency steering demand with a gradually increasing velocity. The methodology shown here describes accurately the lateral forces generated with respect to the tyre slip angle over the entire slip angle operational envelope.

The derived conventional/intelligent vehicle model allows the prediction of lateral velocity, yaw rate, tyre slip angles, tyre forces, and the CG trajectory. The analysis provides an integrated simulation vehicle model which relates the PMDC actuator demands to the robot dynamics.

Vehicle stability issues are directly related to the lateral forces which are generated at the wheel tyre patches. Hence the modelling of these forces is necessary for accurately predicting the vehicle trajectory. For conventional steered vehicles the traditional approach has been used to consider manoeuvres of low to moderate severity. However, there have been attempts to model the vehicle response while the forces approach values near the friction limit at the road/tyre interface. Further work relates the lateral forces to the longitudinal tyre forces using the wheel slip which includes the tyre elasticity properties. In [7] an extension of the LuGre dynamic friction model [8] from longitudinal motion to longitudinal/lateral motion is developed.

In [9] fuzzy logic type-I modelling of vehicles, which are entering the force saturation region, are presented together with experimental results. Two linguistic variables were chosen, hardness and slipperiness which produced a satisfactory tyre-ground interface model.

Other researchers [10] have used a type-I fuzzy logic method to derive the tyre force for a vehicle which has all the wheels driven from a permanent magnet machine.

In the case of a fuzzy tyre model, for fine tuning or even assistance in automatically generating the rules which best describe the tyre lateral force and slip angle surface, several techniques exist in the literature [11–14]. Further research in this area [2] for the class of Takagi–Sugeno–Kang fuzzy systems has related the optimum number of rules and maximum allowed error to the experimental and predicted data.

In this paper, an analytical–linguistic approach has been considered which amalgamates, the physical system in a vehicle dynamics and the fuzzy type-II/III tyre model systems in a "hybrid based method".

In particular the tyre model is a generalised type-III system presented in a fuzzy setting [15].

The proposed approach can be applied to robotic vehicles [16] in which an explicit mathematical lateral tyre model description is available with respect to the front and rear tyre slip angles. One of the advantages of using the fuzzy type-II tyre model, instead of a piecewise linearised model is that the complete lateral force envelope can be studied over the entire front and rear slip angle which can influence the vehicle stability.

The paper is organised as follows: In Section 2 the vehicle formulation is given which includes kinematics, dynamics, the fuzzy type-II tyre model and properties and the traction (PMDC) actuator model. In Section 3 the simulation results are provided which show the state variable variations, the tyre force generation together with the associated tyre sideslip angles, the CG trajectory and the armature actuator voltage. Finally in Section 4 the concluding remarks are given.

2. Basic concepts

2.1. Tyre lateral force generation

The basic tyre-axle-ground system is shown in Fig. 1. In this case the camber angle which is generated by rotating the wheel with respect to the vertical axis from the ground is zero. The tyre is considered to be elastic and therefore flexible.

When a vehicle yaw request is initiated then a turning moment is induced which causes a slip angle to be generated between the hub and the elastic tyre. This angle is usually less than 12 rotational degrees but sufficiently large to cause a smooth rotation compared to a maximum Ackerman vehicle wheel rotation of approximately 30 rotational degrees. The maximum slip angle depends on the friction limit between the tyre and the ground, the tyre elastic characteristics, the tyre pressure and finally on the differential demand between the two wheel sides. Fig. 2 illustrates the tyre slip angle generation. At time $t = \delta t$ the tyre contact patch partially reaches the friction limit and therefore tyre scuffing occurs and the remaining area of the tyre patch temporarily deforms and creates an Ackerman equivalent angle. As the wheel rotates the two combined effects of wheel rolling and tyre deformation cause the overall vehicle to turn smoothly by requesting a differential demand. The tyre force is a complex variable to model due to the large number of conflicting parameters. For example a large patch area would offer less sinkage on a soft surface and therefore reduces losses. It would also cause greater friction for the tyre on hard tarmac grounds and therefore increased difficulty in turning.

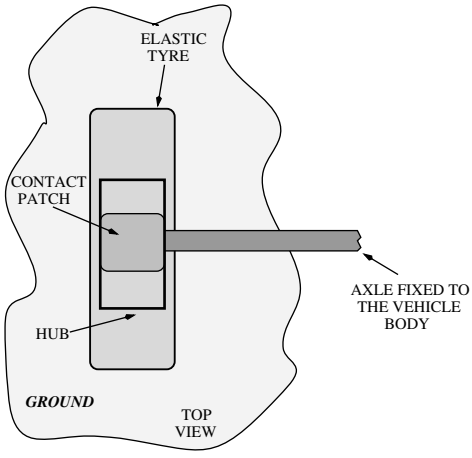

Fig. 1. Basic tyre-axle system (top view).

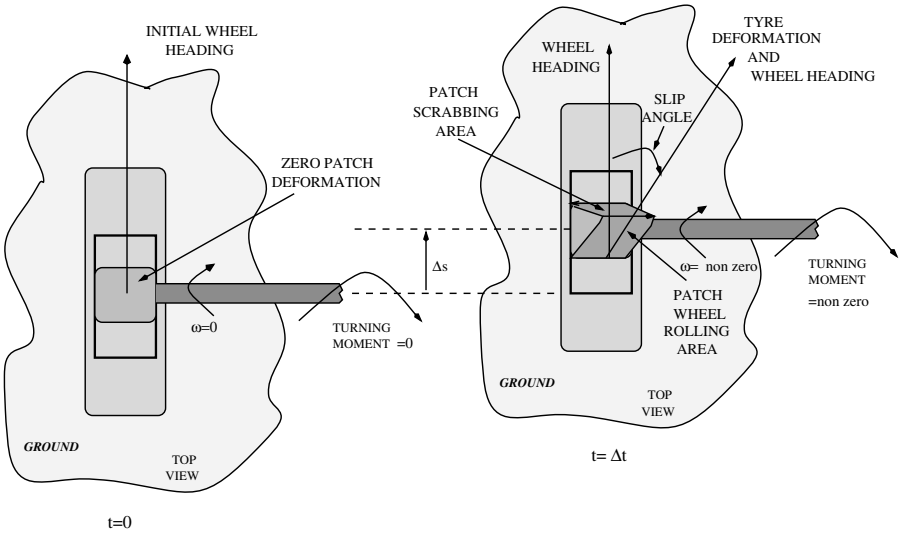

Fig. 2. Wheel slip angle graphical generation.

2.2. Experimental setup

The tyre rig used for obtaining data consisted of a moving road which simulates a free rolling wheel on tarmac, the vertical load system, the tyre slip angle setting, the camber angle setting, and the lateral force transducers as shown in Fig. 3. Firstly the rig was calibrated using the appropriate equipment and after placing the wheel with the required camber and slip angle and vertical load the experiment may start. The rig then provides the induced cornering force in real time and therefore a mapping between the several slip angles and cornering forces for different vertical loads.

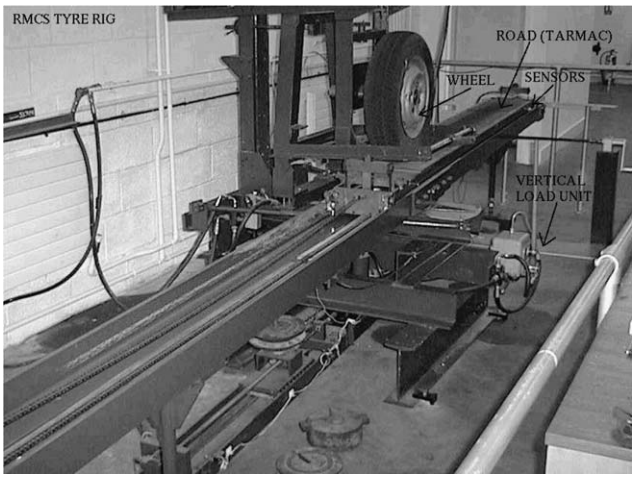

Fig. 3. Tyre-rig at Cranfield University.

3. Part (A): Physical vehicle model formulation

The vehicle forward velocity (u) is considered to be constant (or slowly varying), whilst the lateral velocity (v) and the yaw rate (r) about the CG are the state variables. The vehicle input is the front wheel steering angle while Sienel coefficient of friction [16] are constant. The Ackerman steered vehicle can be modelled by using a single track as shown in Fig. 4. The rear wheels are driven from the PMDC via the step-down gearbox (n_g).

3.1. Wheel kinematics

The front and rear wheel longitudinal and lateral velocity components are given in Eq. (1).

$$\left.\begin{aligned} u_f &= u, \quad v_f = v + l_f r \\ u_r &= u, \quad v_r = v - l_r r \end{aligned}\right\} \tag{1}$$

The vehicle chassis sideslip angles (β_f, β_r) for the front and rear tyres are given in Eq. (2).

$$\left.\begin{aligned} \beta_f &= \arctan\left(\frac{v_f}{u_f}\right) \\ \beta_r &= \arctan\left(\frac{v_r}{u_r}\right) \end{aligned}\right\} \tag{2}$$

The tyre sideslip angles (α_f, α_r) for the front and rear tyres are given in Eq. (3).

$$\left.\begin{aligned} \alpha_f &= \delta - \beta_f \\ \alpha_r &= -\beta_r \end{aligned}\right\} \tag{3}$$

The equations in (3) capture the entire tyre slip angle non-linear envelope rather than small angles. Substitution of Eqs. (1) and (2) in Eq. (3) resulted in Eq. (4).

$$\left.\begin{aligned} \alpha_f &= \delta - \arctan\left(\frac{v + l_f r}{u}\right) \\ \alpha_r &= -\arctan\left(\frac{v - l_r r}{u}\right) \end{aligned}\right\} \tag{4}$$

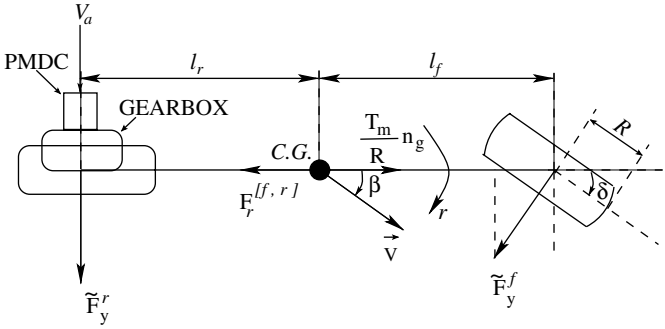

Fig. 4. Single track vehicle schematic.

Eq. (4) relates firstly the front tyre sideslip angle to the steering demand (δ) and the chassis state variables (v, r), the longitudinal velocity (u) and the distance between the CG and the front track (l_f). Secondly the rear front sideslip angle also relates to (v, r, u, l_r).

3.2. Vehicle dynamics

It can be shown that the vehicle Newtonian motion dynamics can be simplified to the Equations in (5) by assuming relatively gradual and small changes in the longitudinal velocity (u) result to ($\dot{u} \approx 0$).

$$\left.\begin{array}{l} \frac{dv(t)}{dt} = \frac{F_y^r}{m} + \frac{F_y^f}{m} - u(t)r(t) \\ \frac{dr(t)}{dt} = F_y^f l_f - F_y^r l_r \end{array}\right\} \tag{5}$$

4. Part (B): Fuzzy type-II and type-III tyre models

In this section the tyre model has been modelled firstly as a generalised type-III fuzzy system which is then reduced to a type-II fuzzy system. The proposed fuzzy type-III tyre model piecewise linear section which corresponds to the fuzzy qth rule is given in Eq. (6).

$$\left.\begin{array}{l} \text{Rule } q \in [2, q_{\max}] : \underbrace{\text{IF } \alpha_{[f,r]} \text{ is } A_q \ldots}_{\text{Fuzzy Antecedent}} \text{ THEN } \underbrace{F_y^{[r,f](q)} = \left.\frac{\partial F_y^{[r,f]}}{\partial \alpha_{[r,f]}}\right|^{(q)} \alpha_{[r,f]} + \gamma^{(q)}}_{\text{Type-III Consequent}} \\ \quad \text{where } q \in N^{*+} \end{array}\right\} \tag{6}$$

The fuzzy logic methodology allows the user to define the regions of linearity from observation or alternatively via the use of clustering tools such as the subtractive clustering method [13,14] or via means of parameter estimation approaches for a priori number of rules. The individual qth fuzzy rule applied here is of a fuzzy type-II and secondly of type-III and therefore each individual rule is a singleton or piecewise linear respectively. The resulting rule blending produces the lateral tyre force which retains the non-linear tyre characteristics. An advantage of type-III fuzzy systems over the type-II fuzzy systems is normally the rule reduction for the same high order nonlinearity according to [17]. The selected continuous Gaussian membership functions are shown in Eq. (7).

$$\left.\begin{array}{l} \mu_{A_q}(\alpha_{[f,r]}, c_q^{[f,r]}, d_q^{[f,r]}) = \Lambda \times e^{\left(\frac{-\left(\alpha_{[f,r]} - c_q^{[f,r]}\right)^2}{d_q^{[f,r]}}\right)} \\ \quad \text{with } q = \text{a priori} \\ q = Q \in [2, m] \\ \Lambda = \max_q \left\{\mu_{A_q}\left(\alpha_{[f,r]}, c_q^{[f,r]}, d_q^{[f,r]}\right)\right\}, \quad \forall q \in Q \\ d_q = 2\sigma^2 \end{array}\right\} \tag{7}$$

where (m) is a positive integer equal to the number of raw data points for the overall experimental tyre data set.

4.1. Fuzzy type-III tyre properties

In this section the fuzzy type-III properties are given which are valid for a tyre which exerts non-linear behaviour.

Property 1. *Fuzzifier*: *Let* $(\alpha_{[f,r]})$ *be objects in the Universes* $\Omega_{\alpha_{[f,r]}} \subset \Omega$. *The fuzzifier is a function which maps the variable* $(\alpha_{[f,r]})$ *to values into interval* $[0,1]$ *with* $\Lambda = 1$ (*normal sets*), *Eq.* (7).

Property 2. *Consistency*: *A set of fuzzy rules is consistent if there are no rules with the same antecedent but different Sugeno consequent.*

Property 3. *Rules completeness*: *A set of fuzzy rules is complete if for any* $(\alpha_{[f,r]}) \in \Omega$ *there exists at least one rule* $q \in [1, q_{\max}]$ *such that* $\mu_{A_q}(\alpha_{[f,r]}) \neq 0$.

Property 4. *Rule influence*: *The qth* $\in [1, q_{max}]$ *rule influence* λ_q *which combines the propositions of the antecedent for each qth rule and is given by*: $\lambda_q = (\prod_{j=1}^{j_{\max}} \mu_{A_q^j}(x_j))_q$. *Where for this application* x_j *for* $j = 1$ *is given by* $\underline{x} \triangleq [x_1] = \alpha_{[f,r]}$.

Property 5. *Membership functions*: *The fuzzy sets for the Sugeno variable are*: $A_q = \{\Omega_{\alpha[f,r]} \subset \Omega \mid \mu_{A_q}(\alpha_{[f,r]})\}$.

Property 6. *The parallel fuzzy firing of all* 1*st order q-rules result to the fusion equation* (8).

$$\left.\begin{aligned} \widetilde{F}_y^{[\mathrm{f,r}]}(\alpha) &= \frac{\sum_{q=1}^{q_{\max}} \lambda_q \left(\dfrac{\partial F_y^{[\mathrm{f,r}]}}{\partial \alpha_{[\mathrm{f,r}]}} \Big|^{(q)} \alpha_{[\mathrm{f,r}]} + \gamma^{(q)} \right)}{\sum_{q=1}^{q_{\max}} \lambda_q} \\ \text{where } \lambda_q &= \prod_{j=1}^{j_{\max}} \mu_{A_q^j}(\alpha_{[\mathrm{f,r}]}) = \mu_{A_q}(\alpha_{[\mathrm{f,r}]}) \\ h &= \sum_{q=1}^{q_{\max}} \lambda_q = 1 \pm \Delta\epsilon \end{aligned}\right\} \tag{8}$$

where $(\Delta\epsilon)$ *is the optimisation error.*

The tyre non-linearity is captured in Eq. (8) because all the piecewise linear models have been fused via the nonlinear membership relationships. For this specific tyre, Eq. (8) is expanded to Eq. (9).

$$\left.\widetilde{F}_y^{[\mathrm{f,r}]}(\alpha) = \lambda_1 \frac{\dfrac{\partial F_y^{[\mathrm{f,r}]}}{\partial \alpha_{[\mathrm{f,r}]}} \Big|^{(1)} \alpha_{[\mathrm{f,r}]} + \gamma^{(1)}}{\sum_{q=1}^{q_{\max}} \lambda_q} + \lambda_2 \frac{\dfrac{\partial F_y^{[\mathrm{f,r}]}}{\partial \alpha_{[\mathrm{f,r}]}} \Big|^{(2)} \alpha_{[\mathrm{f,r}]} + \gamma^{(2)}}{\sum_{q=1}^{q_{\max}} \lambda_q} + \cdots + \lambda_{q_{\max}} \frac{\dfrac{\partial F_y^{[\mathrm{f,r}]}}{\partial \alpha_{[\mathrm{f,r}]}} \Big|^{(q_{\max})} \alpha_{[\mathrm{f,r}]} + \gamma^{(q_{\max})}}{\sum_{q=1}^{q_{\max}} \lambda_q} \right\} \tag{9}$$

The resulting fuzzy type-II lateral force generation is shown in Eq. (10). The non-linear fuzzy type-II augmented coefficients $(\xi_1^{[\mathrm{f,r}]}, \xi_2^{[\mathrm{f,r}]}, \ldots, \xi_{q_{\max}}^{[\mathrm{f,r}]})$ are given in Eq. (11).

$$\left.\widetilde{F}_y^{[\mathrm{f,r}]}(\alpha) = \xi_1^{[\mathrm{f,r}]} + \xi_2^{[\mathrm{f,r}]} + \cdots + \xi_{q_{\max}}^{[\mathrm{f,r}]} \right\} \tag{10}$$

$$\left.\begin{aligned}
\xi_1^{[\mathrm{f,r}]} &= \frac{\mathrm{e}^{\left(\frac{-\left(\alpha_{[\mathrm{f,r}]}-c_1^{[\mathrm{f,r}]}\right)^2}{d_1^{[\mathrm{f,r}]}}\right)}\left(\left.\frac{\partial F_y^{[\mathrm{f,r}]}}{\partial \alpha_{[\mathrm{f,r}]}}\right|^{(1)}\alpha_{[\mathrm{f,r}]}+\gamma^{(1)}\right)}{h}+\\
\xi_2^{[\mathrm{f,r}]} &= \frac{\mathrm{e}^{\left(\frac{-\left(\alpha_{[\mathrm{f,r}]}-c_2^{[\mathrm{f,r}]}\right)^2}{d_2^{[\mathrm{f,r}]}}\right)}\left(\left.\frac{\partial F_y^{[\mathrm{f,r}]}}{\partial \alpha_{[\mathrm{f,r}]}}\right|^{(2)}\alpha_{[\mathrm{f,r}]}+\gamma^{(2)}\right)}{h}\\
&\vdots\\
\xi_{q_{\max}}^{[\mathrm{f,r}]} &= \frac{\mathrm{e}^{\left(\frac{-\left(\alpha_{[\mathrm{f,r}]}-c_{q_{\max}}^{[\mathrm{f,r}]}\right)^2}{d_{q_{\max}}^{[\mathrm{f,r}]}}\right)}\left(\left.\frac{\partial F_y^{[\mathrm{f,r}]}}{\partial \alpha_{[\mathrm{f,r}]}}\right|^{(q_{\max})}\alpha_{[\mathrm{f,r}]}+\gamma^{(q_{\max})}\right)}{h}
\end{aligned}\right\} \tag{11}$$

In Eq. (12) the coefficient is always greater than zero thus guaranteeing constraint force levels hence $g > 0$ which is a direct result of rules completeness fuzzy Property 3.

$$\left.h = \mathrm{e}^{\left(\frac{-\left(\alpha_{[\mathrm{f,r}]}-c_1^{[\mathrm{f,r}]}\right)^2}{d_1^{[\mathrm{f,r}]}}\right)}+\mathrm{e}^{\left(\frac{-\left(\alpha_{[\mathrm{f,r}]}-c_2^{[\mathrm{f,r}]}\right)^2}{d_2^{[\mathrm{f,r}]}}\right)}+\cdots+\mathrm{e}^{\left(\frac{-\left(\alpha_{[\mathrm{f,r}]}-c_{q_{\max}}^{[\mathrm{f,r}]}\right)^2}{d_{q_{\max}}^{[\mathrm{f,r}]}}\right)}>0\right\} \tag{12}$$

Eq. (12) for $\left.\frac{\partial F_y^{[\mathrm{f,r}]}}{\partial \alpha_{[\mathrm{f,r}]}}\right|^{(q)}=0,\ \forall q \in Q$ reduces to a type-II system with force coefficients given from Eq. (13).

$$\left.\begin{aligned}
\varphi_1^{[\mathrm{f,r}]} &= \frac{\mathrm{e}^{\left(\frac{-\left(\alpha_{[\mathrm{f,r}]}-c_1^{[\mathrm{f,r}]}\right)^2}{d_1^{[\mathrm{f,r}]}}\right)}}{h}(\gamma^{(1)})+\\
\varphi_2^{[\mathrm{f,r}]} &= \frac{\mathrm{e}^{\left(\frac{-\left(\alpha_{[\mathrm{f,r}]}-c_2^{[\mathrm{f,r}]}\right)^2}{d_2^{[\mathrm{f,r}]}}\right)}}{h}(\gamma^{(2)})\\
&\vdots\\
\varphi_{q_{\max}}^{[\mathrm{f,r}]} &= \frac{\mathrm{e}^{\left(\frac{-\left(\alpha_{[\mathrm{f,r}]}-c_{q_{\max}}^{[\mathrm{f,r}]}\right)^2}{d_{q_{\max}}^{[\mathrm{f,r}]}}\right)}}{h}(\gamma^{(q_{\max})})
\end{aligned}\right\} \tag{13}$$

According to [17] the type-II is a special case of type-III and type-I fuzzy systems. For the vehicle application the optimisation results captured the tyre non-linearity for both fuzzy settings,i.e. type-II and type-III systems. For the type-II systems $h \in \Re^{*+}$. For the type-III fuzzy setting it was possible in addition to the good agreement between the fuzzy output and experimental results to constrain $h \cong 1$ and therefore simplify the defuzzification function.

The reduced fuzzy type-II tyre model singleton description which corresponds to the fuzzy qth rule is given in Eq. (14).

$$\left.\text{Rule } q \in [2, q_{\max}] : \underbrace{\text{IF } \alpha_{[\mathrm{f,r}]} \text{ is } A_q \ldots}_{\text{Fuzzy Antecedent}} \text{ THEN } \underbrace{F_y^{[r,f](q)} = \gamma^{(q)}}_{\text{Type-II Consequent}} \quad \text{where } q \in N^{*+}\right\} \tag{14}$$

For the fuzzy type-II problem formulation the properties in Section 4.1 are valid with the exception of property (8) which reduces to property:

Property 7. *The parallel fuzzy firing of the singleton q-rules result to the fusion equation (15).*

$$\left.\begin{aligned} \widetilde{F}_y^{[\mathrm{f,r}]}(\alpha) &= \frac{\sum_{q=1}^{q_{\max}} \lambda_q(\gamma^{(q)})}{\sum_{q=1}^{q_{\max}} \lambda_q} \\ \text{where } \lambda_q &= \prod_{j=1}^{j_{\max}} \mu_{A_q^j}(\alpha_{[\mathrm{f,r}]}) = \mu_{A_q}(\alpha_{[\mathrm{f,r}]}) \\ h &= \sum_{q=1}^{q_{\max}} \lambda_q \in \Re^{+*} \end{aligned}\right\} \tag{15}$$

4.2. Multi-objective type-II and type-III problem formulations

The number of rules (q) are a priori. For every additional rule per fuzzy variable there will be two additional parameters, the membership function spread and centre. The schematic in Fig. 5 summarises the fuzzy logic based procedure.

For the three rule problem setting the objective function for the type-II is shown in (16).

$$\min_{[c_q,d_q,\gamma^q]} \sum_{\tau=1}^{m} \left(\widetilde{F}_y^{[\mathrm{f,r}]}\Big|_{\mathrm{EXP}}^{\tau} - \widetilde{F}_y^{[\mathrm{f,r}]}\Big|_{\text{type-II}}^{\tau} \right)^2 \quad \forall q \in Q \tag{16}$$

where (m) is the number of data points. Equation results into the estimation of nine parameters $[c_q, d_q, \gamma^q]$ with a $q = 3$. In particular parameters $[c_q, d_q] =$ are for the qth membership function and parameters $[\gamma^q] =$ are for the qth singleton consequent.

For the three rule problem setting the objective function for the type-III is shown in (17).

$$\min_{[c_q,d_q,\beta^q,\gamma^q]} \left\{ \left(w_1 \sum_{\tau=1}^{m} \left(\widetilde{F}_y^{[\mathrm{f,r}]}\Big|_{\mathrm{EXP}}^{\tau} - \widetilde{F}_y^{[\mathrm{f,r}]}\Big|_{\text{type-III}}^{\tau} \right)^2 \right) + w_2 \sum_{\tau=1}^{m} (\Gamma^{\tau})^2 \right\} \quad \forall q \in Q \tag{17}$$

where (w_1, w_2) are the normalisation indices. Also $\frac{\partial F_y^{[\mathrm{f,r}]}}{\partial \alpha_{[\mathrm{f,r}]}}\Big|^q = \beta^q$. (Γ^{τ}) is given from Eq. (18).

$$\forall \tau \in [1, m] \Gamma^{\tau} = 1 - Den\left(\widetilde{F}_y^{[\mathrm{f,r}]}\Big|_{\text{type-III}}^{\tau} \right) \tag{18}$$

Eqs. (17) and (18) results into the estimation of 12 parameters $[c_q, d_q, \beta^q, \gamma^q]$ for $q = 1, 2, 3$. In particular parameters $[c_q, d_q] =$ are for the qth membership function and parameters $[\beta^q, \gamma^q] =$ are for the qth piecewise linear consequent. The parameter estimation results are shown for both cases type-II and type-III systems in Figs. 11 and 12.

4.3. Proposed fuzzy-hybrid structure

The theoretical fuzzy-hybrid structure is shown in Eq. (19). The function consists of two parts. Firstly the physical system modelling part and secondly the fuzzy type-III part.

$$y = F(\underline{\mathbf{u}}, \underline{\mathbf{p}}, \mathscr{H}) \tag{19}$$

where

y	model output
F	fuzzy-hybrid non-linear equation

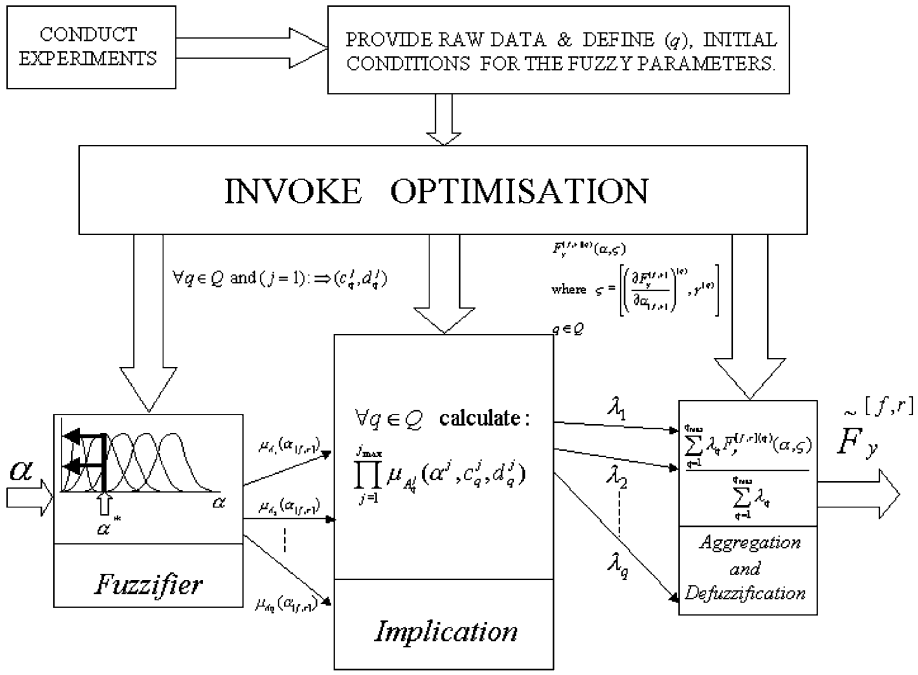

Fig. 5. Part (b): Optimisation with $q =$ a priori for estimating the membership function properties (consequents parameters) for type-II and type-III systems.

$\underline{\mathbf{u}}$	model input vector
$\underline{\mathbf{p}}$	$[\underline{p}_a, \underline{p}_b, \underline{p}_c \ldots]$ parameter vector
$\underline{p}_a$	parameter vector for sub-system (a)
$\underline{p}_b$	parameter vector for sub-system (b)
$\underline{p}_c$	parameter vector for sub-system (c)
$\mathscr{H}$	type-III fuzzy expression

In particular the non-linear function F is defined from Eq. (20).

$$y = f_1(\underline{\mathbf{p}})u_1 + f_2(\underline{\mathbf{p}})g(u_2)\mathscr{H} + f_3(\underline{\mathbf{p}}) \tag{20}$$

where

f_z	lumped parameter vector $\forall z = [1,3]$
$g(u_2)$	non-linear input function for input 2

Eq. (20) can be rearranged to Eq. (21).

$$y = \underbrace{\overbrace{f_1(\underline{\mathbf{p}})u_1 + f_3(\underline{\mathbf{p}}) + f_2(\underline{\mathbf{p}})g(u_2)}^{\text{Physical system model}} \quad \underbrace{\mathscr{H}}_{\text{Fuzzy type-III model}}}_{\text{Fuzzy-Hybrid model}} \tag{21}$$

The proposed fuzzy-hybrid structure is shown in Fig. 6.

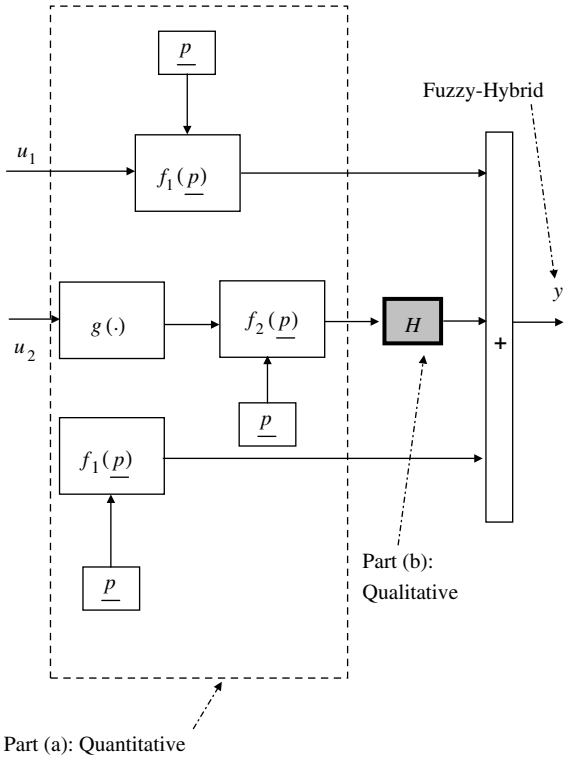

Fig. 6. The fuzzy-hybrid generic block diagram.

4.4. Hybrid modelling: physical system and fuzzy interface

4.4.1. Sienel and fuzzy tyre model

The lateral tyre force components along the vehicle axis are modelled using the front and rear fuzzy type-II and type-III cornering forces $(\widetilde{F}^{\mathrm{f}}_{y}(\alpha_{\mathrm{f}}), \widetilde{F}^{r}_{y}(\alpha_{\mathrm{r}}))$ as shown in Eq. (22):

$$\left.\begin{aligned} F^{\mathrm{f}}_{y} &= \mu_{\mathrm{f}}\widetilde{F}^{\mathrm{f}}_{y}(\alpha_{\mathrm{f}})\cos(\delta) \\ F^{r}_{y} &= \mu_{\mathrm{r}}\widetilde{F}^{r}_{y}(\alpha_{\mathrm{r}}) \end{aligned}\right\} \tag{22}$$

where $(\mu_{\mathrm{f}}, \mu_{\mathrm{r}})$ are the Sienel surface anisotropic coefficients [16] which correspond to a scaling of the fuzzy type-II non-linear surfaces. The Sienel coefficients can represent a dry tarmac surface or even an icy surface. The fuzzy type-II lateral force modelling captures the entire skidding envelope from relatively small tyre slip angles (linear cornering coefficient) up to angles which cause the lateral force to saturate and decrease for any further increase of the tyre slip angles (non-linear behaviour). In the literature there are several references which are addressing the tyre modelling issues in mainly a conventional manner.

In this paper, however, (Fig. 7) the authors have proposed a fuzzy logic type-II model for the lateral tyre forces model for use in vehicle based on experimental tyre data rather than overall vehicle data. The Sugeno fuzzy model has been optimised by means of using

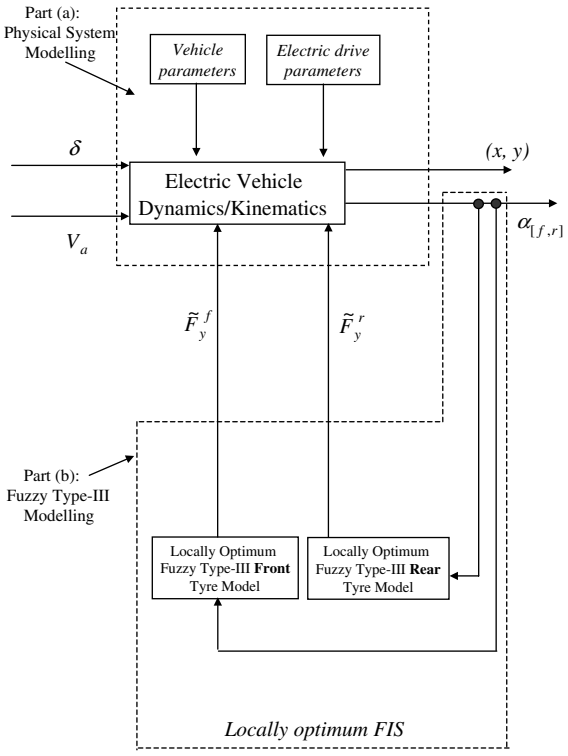

Fig. 7. The hybrid concept block diagram for the electric vehicle application.

the subtractive clustering method as was firstly introduced in [13] and applied to the case of a differentially steered vehicle in [18].

5. Experimental results

The data acquired provided the dynamic tyre cornering force and the distance travelled by the wheel. Fig. 8 shows the experimental data which were obtained from the tyre rig for different tyre slip angles. The wheel rolls at a constant speed while the slip angle is set initially by varying the travelling surface with respect to the hub heading. Fig. 8 shows that as the tyre slip angle increases with the cornering force, which has been converted to the wheel lateral force.

However for the fuzzy type-II and type-III model analysis the steady-state data were obtained by considering the data set $\mathscr{Z}_i \subset \mathscr{P}_i$ where $\mathscr{P}_i$ represents the dynamic data set for each tyre slip angle $\alpha_i = \{1°, 3°, 5°, 7°, 9°\}$. The steady-state data sets $\mathscr{Z}_i$ were extracted from Fig. 8 and are shown in Fig. 9.

The resulting combined experimental data set $\mathscr{Z} = \{\mathscr{Z}_1 \cup \mathscr{Z}_3 \cup \mathscr{Z}_5 \cup \mathscr{Z}_7 \cup \mathscr{Z}_9\}$ is shown in Fig. 10.

The experimental data sets were used for the optimisation type-II and type-III problem formulations. The results have been summarised in Figs. 11 and 12.

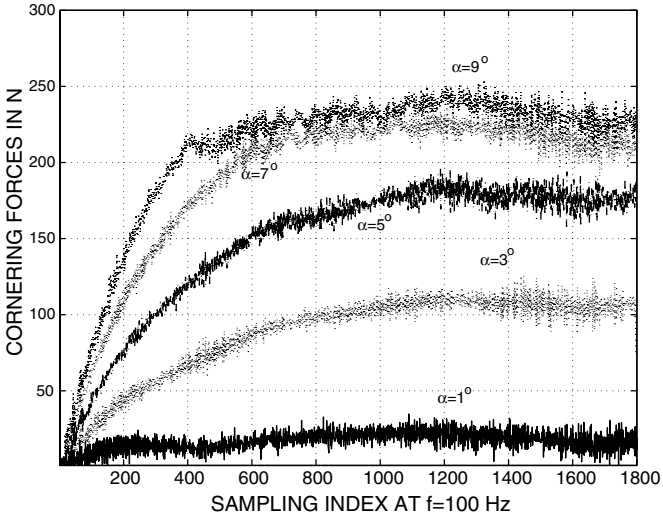

Fig. 8. Experimental data obtained from the tyre rig for different tyre slip angles (f = sampling frequency).

Fig. 11 shows the estimated membership functions centres and spreads. The type-II system for the same experimental data resulted in three rules significantly influencing the output per time instant. Therefore the α-*cuts* are not necessarily well defined and as a result the estimated fused type-II denominator output is not normal, and the defuzzification denominator varies between [1,3]. The three type-II singletons are positioned at the membership function centres. Finally, Fig. 11 shows the estimated type-II force which is in good agreement when compared to the experimental data sets.

The type-II tyre fuzzy sub-system had the following term $\sum_{q=1}^{q_{\max}} \lambda_q$ unconstrained and hence this resulted in α-*cuts* which where other than 50%. Hence the resulting type-II membership functions $A_q(\alpha)$ although there are normal sets they where producing a rather nonlinear behavior over the tyre-slip angle range in order to compensate the singleton fuzzy consequents. Normally type-II systems for the same number of rules when compared to a type-III representation for the same set of experimental data exhibit fuzzy antecedent which are dominating a wider membership function spread. Hence when all fuzzy type-II rules are triggered per time interval (but at a different degree), and fused these result in the required non-linear tyre behavior.

Type-II systems however due to the complex antecedent membership functions although the provide a useful and comprehensive output for these physical sub-system, they do not guarantee logical qualitative explanation of the fuzzy sub-model itself. For a type-II fuzzy tyre representation to become more useful from a qualitative point of view there was a compromise in the estimate tyre force and hence impractical for the purpose of this paper.

Type-III fuzzy representations did however offer great advantages over the type-II representation. In particular Fig. 12 shows the type-III parameter estimation results. Part of the optimisation problem formulation was to retain the α-*cuts* = 0.5. The fuzzy output nonlinear denominator is unity within a small error bound which was expected as part of the optimisation. The piecewise linear type-III equations are also shown together with

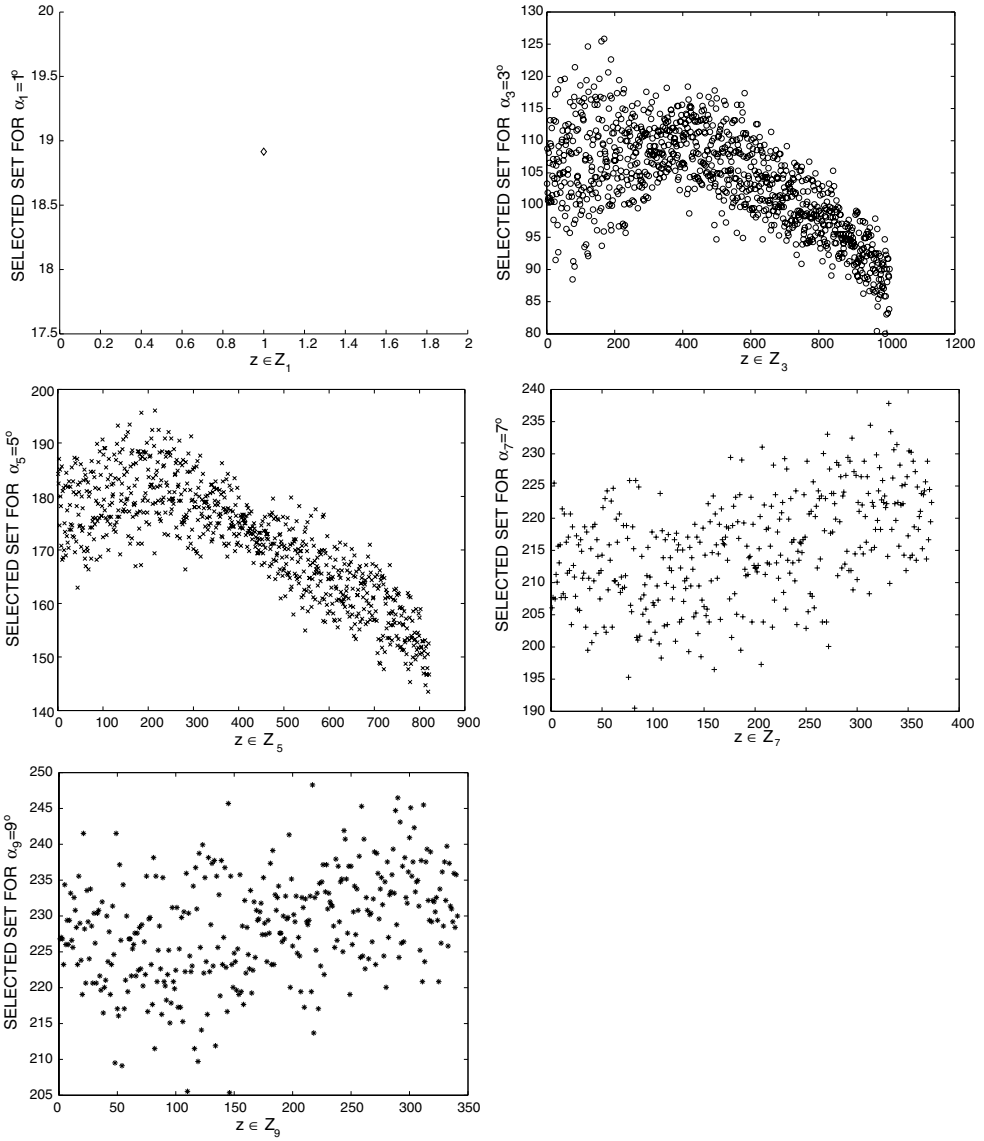

Fig. 9. Reduced experimental $\mathscr{Z}_i$ tyre data sets for $\alpha = \{1,3,5,7,9\}°$.

their side-bar graph tyre slip-angle range of influence. Finally the output fuzzy type-III results show a good agreement when compared to the experimental data while equally importantly retaining a logical qualitative and quantitative output.

Both type-II and type-III fuzzy output results provide good quantitative results similar to these with look-up tables or regression models. However the type-III problem formulation with the constrained multi-objective parameter estimation has resulted to well-defined membership function spaces which preserve the qualitative advantage of fuzzy

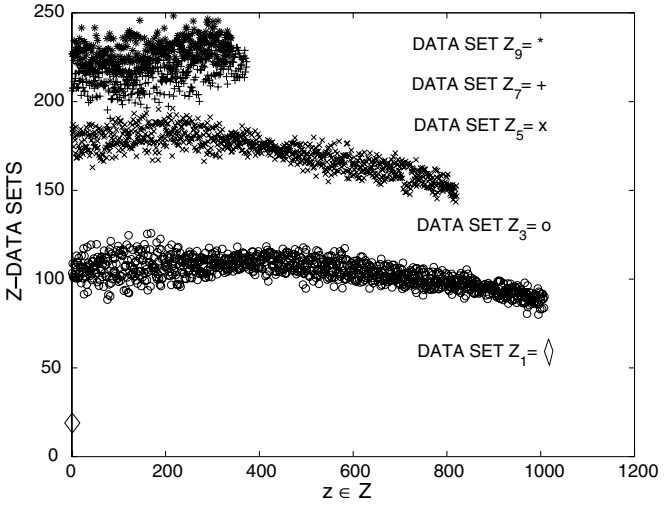

Fig. 10. Union of the reduced experimental data sets $\mathscr{Z}_i$.

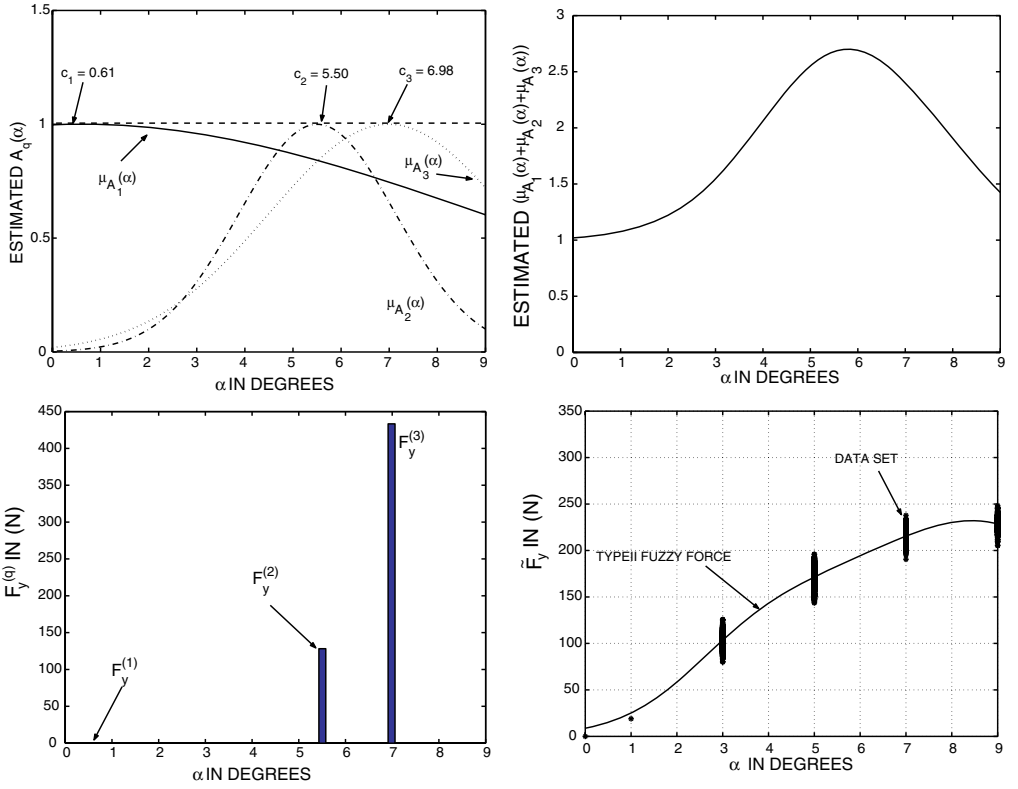

Fig. 11. Membership functions, type-II denominator, type-II outputs and fuzzy fused type-II estimated force.

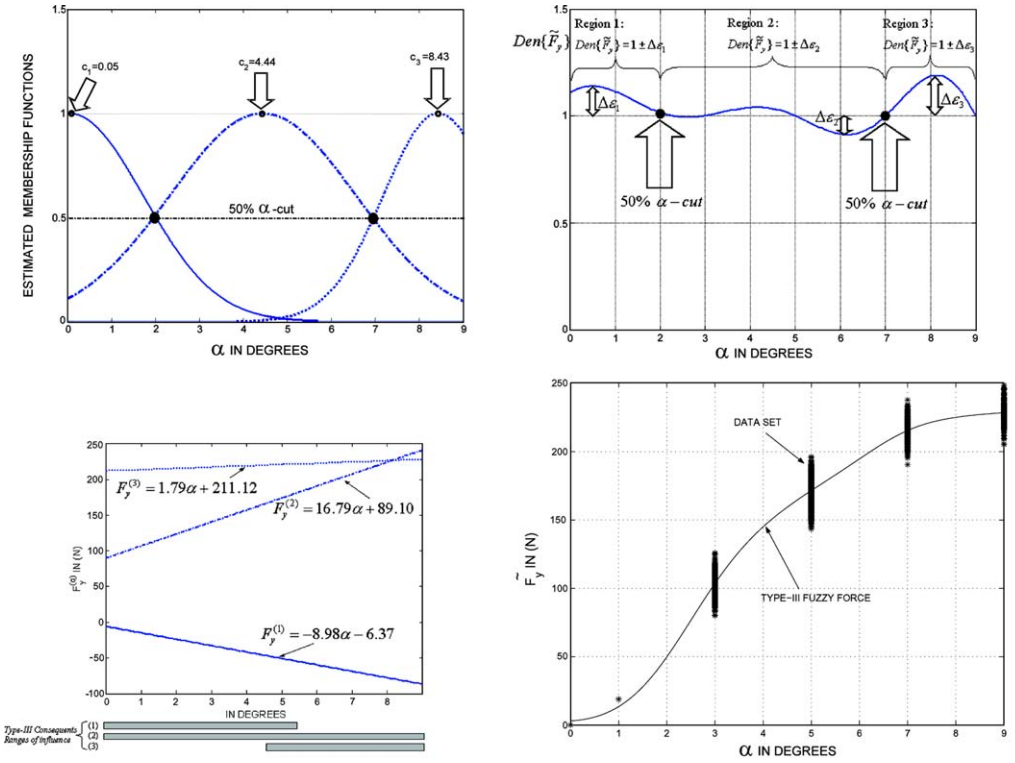

Fig. 12. Membership functions, type-III denominator, type-III outputs and fuzzy fused type-III estimated force.

Table 1
Type-III membership function and linguistic map allocation

Membership function 1	$A_1(\alpha_{[f,r]})$	$\triangleq$	'SMALL'
Membership function 2	$A_2(\alpha_{[f,r]})$	$\triangleq$	'MEDIUM'
Membership function 3	$A_3(\alpha_{[f,r]})$	$\triangleq$	'LARGE'

Table 2
Fuzzy sub-system type-III rule base

Rule index	Antecedent	$\Rightarrow$	Consequent
Rule 1	IF $\alpha(t)$ is SMALL	THEN	$F_y^{(1)}(t) = -8.98\alpha(t) - 6.37$
Rule 2	IF $\alpha(t)$ is MEDIUM	THEN	$F_y^{(2)}(t) = 16.79\alpha(t) + 89.10$
Rule 3	IF $\alpha(t)$ is LARGE	THEN	$F_y^{(3)}(t) = 1.79\alpha(t) + 211.12$

logic systems. This allows an analyst to assess a particular model from both the qualitative and quantitative points of view within the context of hybrid-fuzzy framework.

The membership function allocation table for the type-III fuzzy representation is shown in Table 1.

Table 2 demonstrates that a small number of rules, in this case three, is sufficient to provide effective results which can be assessed from both the qualitative and quantitative point of view.

The strength of the fuzzy-hybrid approach is that the type-III rule consequents are 'all' activated but to a different degree when compared to other regression methods (for every time instant). Hence for each time instant each rule contributes towards the final crisp output. Generally, regression models although simple to implement, are very sensitive to parameter variations especially during a 'hard' switching mode of operation. In this paper the type-III system approach is in effect a form of fused solution of several regression models which relate to a linguistic problem definition.

As the fuzzy-hybrid model evolves the analyst can view which rules activate and also observe the numbers evolving. Thus providing a qualitative and quantitative solution.

Figs. 13 and 14 show the dynamic activation of the type-II and type-III fuzzy-hybrid models. In particular Fig. 13 show the individual membership function activation 'or influence'. The first three graphs in Fig. 13 shows that for the type-II system representation the first membership function is the dominant throughout the 9 s interval. Membership functions (2, 3) are mainly effective during three instances (4.5 s, 6.2 s, 7.5 s). In Fig. 13 the last three graphs for the type-III representation indicate a more blended membership function contribution. Thus rules one and two in this case for the specific scenario are more effective with rule 3 being effective during the (7 s). For this application type-III systems indicate an improved and more consistent membership function triggering due to the optimisation constraint of 50% α-*cut*.

Fig. 14 shows for both the type-II and type-III sub-model representations the membership function activation with reference to the tyre slip angle variation.

5.1. Ackerman wheeled vehicle

The traction motor effort can be determined by recursive calculation of the induced front wheel longitudinal force (F_x^{f}) (along the vehicle wheelbase), due to the tyre sideslip angle (a_{f}) and the total rolling resistive force $F_{\mathrm{r}}^{[\mathrm{f,r}]}$ [19].

$$\left.\begin{aligned} F_x^{\mathrm{f}} &= \mu_{\mathrm{f}} \widetilde{F}_y^{\mathrm{f}} \sin(\delta) \\ F_{\mathrm{r}}^{[\mathrm{f,r}]} &= K_{\mathrm{r}} mg \end{aligned}\right\} \tag{23}$$

The total longitudinal vehicle force along the vehicle wheelbase is given from Eq. (24). The aerodynamic resistance has not been included simply because it has a very small effect at relatively low to medium velocities [19]. However, the combined effect of the rolling resistance and the cornering force component longitudinal force has been included.

$$F_x = F_x^{\mathrm{f}} + F_{\mathrm{r}}^{[\mathrm{f,r}]} = \mu_{\mathrm{f}} \widetilde{F}_y^{\mathrm{f}} \sin(\delta) + K_{\mathrm{r}} mg \tag{24}$$

The motor supplied torque and angular velocity is given from Eq. (25). These are valid for slow variations of the longitudinal velocity (u).

$$\left.\begin{aligned} T_m &= \frac{F_x R}{n_{\mathrm{g}}} \\ \omega_m &= \frac{u n_{\mathrm{g}}}{R} \end{aligned}\right\} \tag{25}$$

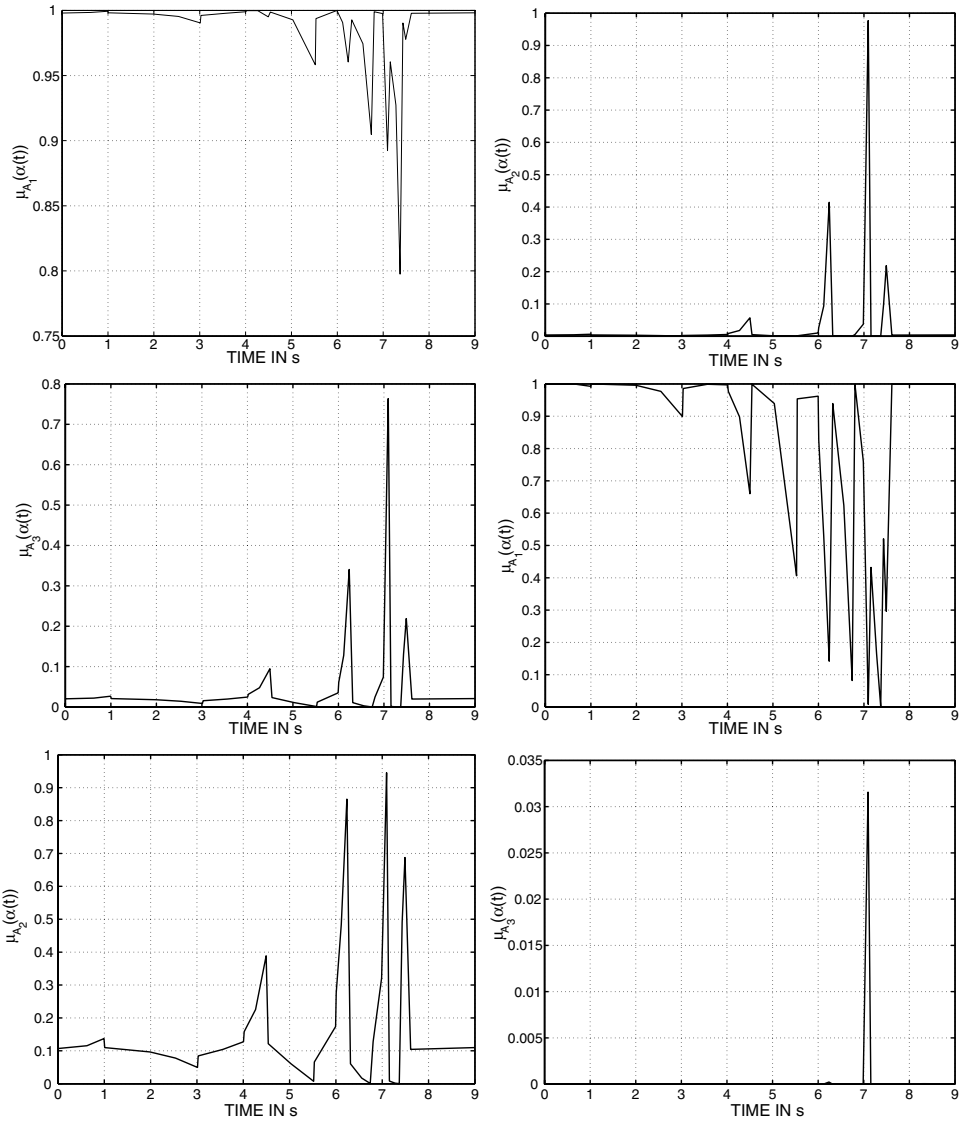

Fig. 13. Membership function dynamic activation for the type-II (first three graphs) and type-III (last three graphs) designs relative to time.

Substitution of Eq. (25) in the equation which describes the PMDC motor with negligible armature inductance results in Eq. (26).

$$V_{\mathrm{a}} = K_{\mathrm{a}} \frac{u n_{\mathrm{g}}}{R} + \frac{R_{\mathrm{a}}}{K_{\mathrm{T}}} \frac{F_x R}{n_{\mathrm{g}}} \tag{26}$$

Finally substitution of Eq. (24) in Eq. (26) results in Eq. (27).

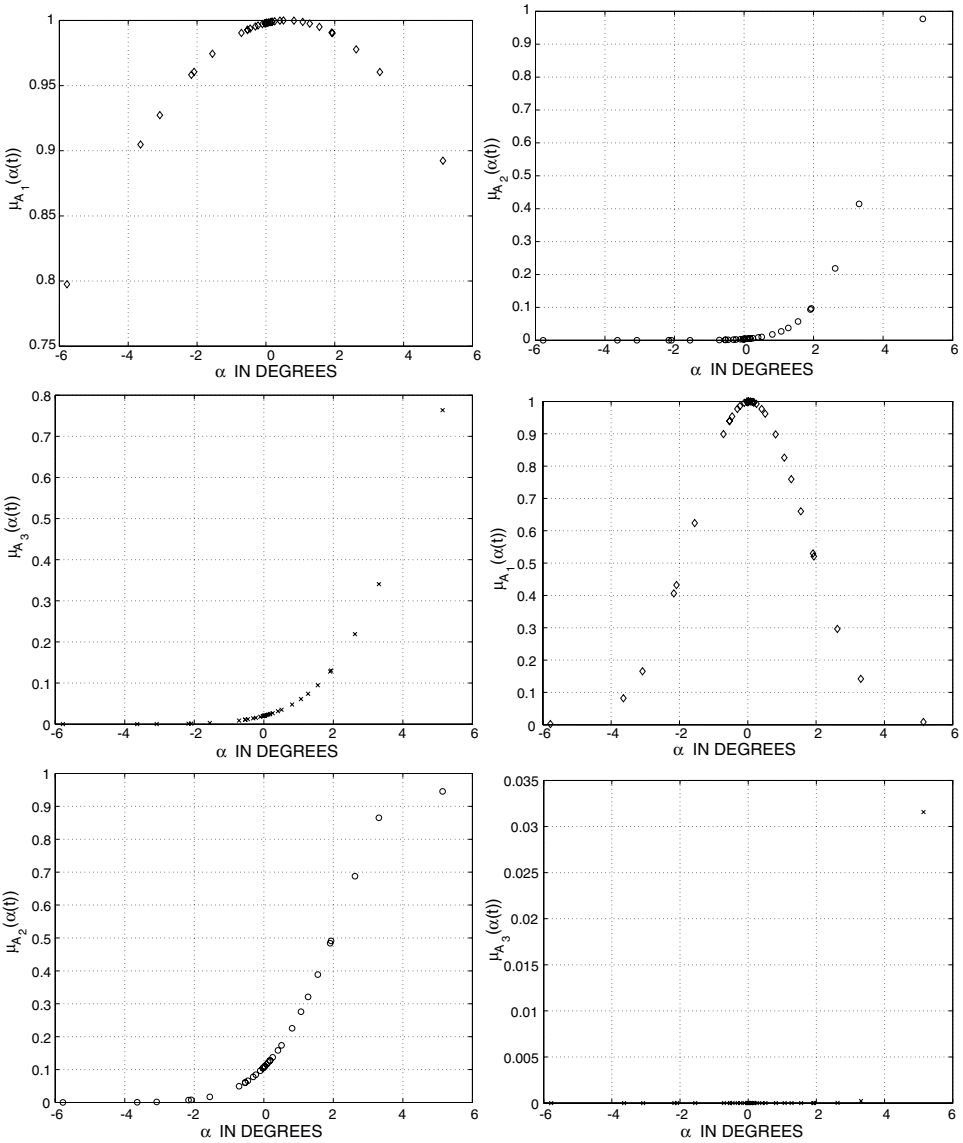

Fig. 14. Membership function dynamic activation for the type-II (first three graphs) and type-III (last three graphs) designs relative to the slip angle effect.

$$V_{\mathrm{a}} = K_{\mathrm{a}} \frac{u n_{\mathrm{g}}}{R} + \frac{R_{\mathrm{a}}}{K_{\mathrm{T}}} \frac{(\mu_{\mathrm{f}} \widetilde{F}^{\mathrm{f}}_{y}(\alpha_{\mathrm{f}}) \sin(\delta) + K_{\mathrm{r}} m g) R}{n_{\mathrm{g}}} \tag{27}$$

Eq. (27) solved for (u) results to Eq. (28).

$$u = \frac{R}{K_{\mathrm{a}} n_{\mathrm{g}}} V_{\mathrm{a}} - \frac{R_{\mathrm{a}} R^2 K_{\mathrm{r}} m g}{K_{\mathrm{a}} n_{\mathrm{g}}^2 K_{\mathrm{T}}} - \frac{R_{\mathrm{a}} R^2 \mu_{\mathrm{f}}}{K_{\mathrm{a}} n_{\mathrm{g}}^2 K_{\mathrm{T}}} \sin(\delta) \widetilde{F}^{[\mathrm{f,r}]}_{y}(\alpha) \quad \text{valid for } u \geqslant 0 \tag{28}$$

Eq. (29) results after combining in Eq. (28) the fuzzy type-III force Eq. (27).

$$\left.\begin{aligned}
&\text{Fuzzy-Hybrid Model Description}\\
&u = \underbrace{\frac{R}{K_a n_g} V_a - \frac{R_a R^2 K_r m g}{K_a n_g^2 K_T} - \frac{R_a R^2 \mu_f}{K_a n_g^2 K_T} \sin(\delta)}_{\text{Physical System Model}} \times \underbrace{\frac{\sum_{q=1}^{q_{\max}} \lambda_q \left(\frac{\partial F_y^{[f,r]}}{\partial \alpha_{[f,r]}} \Big|^{(q)} \alpha_{[f,r]} + \gamma^{(q)} \right)}{\sum_{q=1}^{q_{\max}} \lambda_q}}_{\text{Optimised Fuzzy type-III System}}\\
&\quad \text{where } \lambda_q = \prod_{j=1}^{j_{\max}} \mu_{A_q^j}(\alpha_{[f,r]}) = \mu_{A_q}(\alpha_{[f,r]})\\
&h = \sum_{q=1}^{q_{\max}} \lambda_q \in \Re^{+*}
\end{aligned}\right\} \tag{29}$$

Eq. (29) is of the form of Eq. (21). Comparison of the equations results in the following equivalent terms:

$$\begin{aligned}
&y = u\\
&u_1 = V_a\\
&u_2 = \delta\\
&\underline{p} = [p_a, p_b]\\
&p_{\underline{a}} = [n_g, \mu_f, K_r, m, g, R]\\
&\text{vehicle parameters}\\
&p_{\underline{b}} = [R_a, K_a, K_T]\\
&\text{motor parameters}\\
&f_1(\underline{p}) = \frac{R}{K_a n_g}\\
&f_2(\underline{p}) = \frac{-R_a R^2 \mu_f}{K_a n_g^2 K_T}\\
&f_3(\underline{p}) = \frac{-R_a R^2 K_r m g}{K_a n_g^2 K_T}\\
&H = \frac{\sum_{q=1}^{q_{\max}} \lambda_q \left(\frac{\partial F_y^{[f,r]}}{\partial \alpha_{[f,r]}} \Big|^{(q)} \alpha_{[f,r]} + \gamma^{(q)} \right)}{\sum_{q=1}^{q_{\max}} \lambda_q}
\end{aligned} \tag{30}$$

6. Fuzzy-hybrid modelling results

The vehicle was simulated for a triangular step decrease in frequency waveform with an amplitude of $\delta_{\max} = 35°$ as shown in Fig. 15. During the first four periods (T_1, T_2, T_3, T_4) the waveform was triangular shaped. However during the last fifth period (T_5) no steering

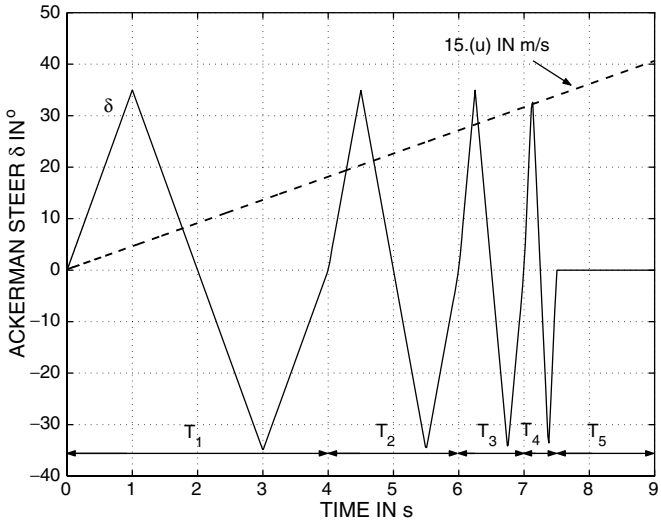

Fig. 15. Test steering input (δ) and demanded longitudinal velocity.

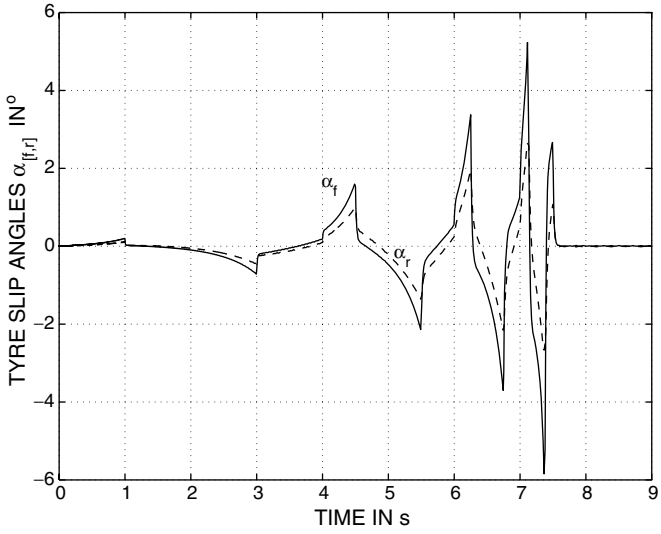

Fig. 16. Vehicle front and rear tyre sideslip angles ($\alpha_{[f,r]}$).

was demanded. During the tested 9*s* time interval the longitudinal velocity was allowed to gradually increase as shown in the scaled-up 15 times as shown in the waveform of Fig. 15.

The fuzzy type-III generated tyre sideslip angles shown in Fig. 16 increase in amplitude as the steering frequency increases.

During these vehicle high steering demands the lateral forces for the front and rear tyres reach high values especially when the steer waveform frequency increases as shown in Fig. 17. The resulting lateral forces follow the sideslip angle variations.

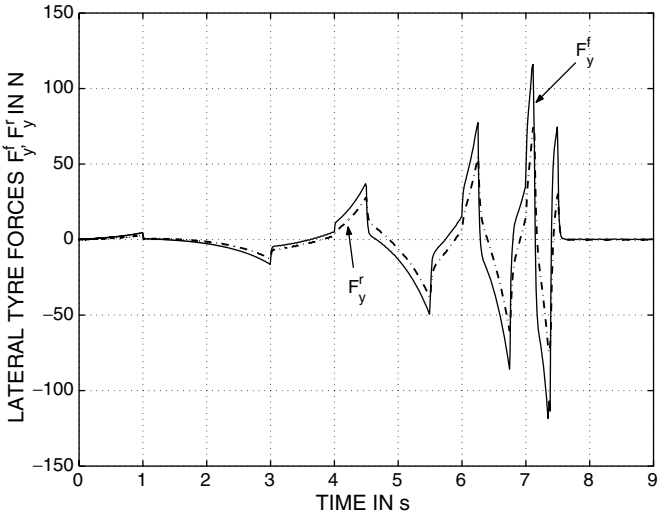

Fig. 17. Vehicle tyre lateral forces ($F_y^{[f,r]}$).

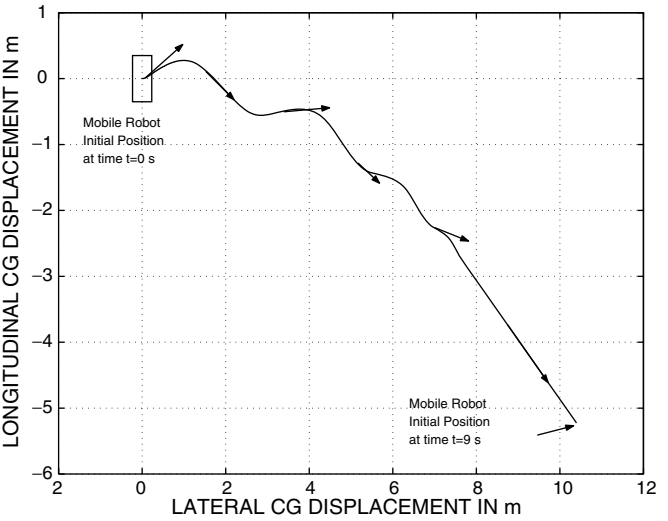

Fig. 18. Vehicle CG trajectory.

The vehicle CG trajectory is shown in Fig. 18 where it may be seen that as the velocity gradually increases it demands higher frequency turns which result to less turning.

7. Conclusions

In this paper, a novel combination of fuzzy type-III and physical system modelling has been presented within a 'hybrid' systems framework. In particular, the model has been

divided into two paradigms: the physical modelling sub-system and the fuzzy type II or III fuzzy sub-systems. The advantages of the type-III system over the type-II system have been discussed. The physical model used conventional and known parameter settings while for the fuzzy sub-system experimental data sets were available for this particular application. The data sets, together with the proposed type-III structure were locally optimised. The resulting overall hybrid model resulted in a system which could be described in a qualitative and quantitative framework, thus, resulting in a better understanding of any subsystem and its effect on the overall model. The proposed methodology allowed the successful synergy of two well accepted and researched methods.

The method was tested on an all-electric vehicle. The analysis shown here allowed prediction of the vehicle characteristics including the planar trajectory by means of the strategic fusion dynamics/kinematics (physical system modelling) and fuzzy based methods such as fuzzy type-II and type-III methodologies. The proposed fuzzy models captured the tyre non-linear characteristics while the conventional methods captured the chassis and actuator dynamics and wheel kinematics. The methodology allowed the capture of the tyre force localised data instead of the global vehicle data, thus minimising hardware development time and cost. Finally, the wheeled vehicle was simulated with increasing frequency steering demand and a gradual increase in the forward velocity. This allowed investigation of the state variables and tyre forces and indicates the strengths for this methodology.

Acknowledgements

The authors would like to thank members of staff from the Engineering System Department from Cranfield University for their availability and assistance during the data capturing phase.

References

[1] U. Kaymak, R. Babuska, Compatible cluster merging for fuzzy modelling, IEEE Proceedings (1995) 897–904.
[2] M. Sami Fadali, A. Sonbol, A new approach for designing TSK fuzzy systems, in: Proceedings 2002 American Control Conference, Anchorage, AK, May, 2002.
[3] R. Babuska, A. Ollero, G. Ulivi, F. Cuesta, in: H.B. Verbruggen, H.J. Zimmermann (Eds.), Fuzzy Logic Applications in Mobile Robotics, Kluwer Academic Publishers, Berlin, 1999.
[4] C.J. Harris, Z.Q. Wu, Neurofuzzy state estimators and their applications, in: Proceedings IFAC Symposium on AI in Real Time Control, vol. 2, 1997, pp. 7–16.
[5] C.J. Harris, M. Brown, K.M. Bossley, D.J. Mills, M. Feng, Advances in neurofuzzy algorithms for real-time modelling and control, Journal of Engineering Application of AI (1996) 1–16.
[6] A.E.B. Ruano, J.M. Lima, A.B. Azevedo, N.M. Duarte, P.J. Fleming, Automatic tuning of controllers using a neural-genetic system, in: Proceedings of the 14th World Congress of International Federation of Automatic Control (IFAC '99), Beijing, July 1999, pp. 7–12.
[7] C. Canudas-de-Wit, E. Velenis, P. Tsiotras, Extension of the Lugre dynamic tire friction model to 2d motion, in: Proceedings of the 10th Mediterranean Conference on Control and Automation—MED2002 Lisbon, Portugal, July 9–12, 2002.
[8] C. Canudas de Wit, Comments on new model for control of systems with friction, IEEE Transactions on Automatic Control 43 (8) (1998).
[9] R.E. Colyer, J.T. Economou, Modelling of skid steering and fuzzy logic vehicle ground interaction, in: Proceedings of the American Control Conference, Chicago, IL, June 2000.

[10] J.T. Economou, Fuzzy logic force modelling, in: Proceedings of the American Control Conference, Anchorage, AK, May, 2002.
[11] R. Babuska, U. Kaymak, Compatible cluster merging for fuzzy modelling, IEEE Proceedings 24 (1995) 897–904.
[12] M.A. Vila, A.F. Gomez-Skarmeta, M. Delgado, About the use of fuzzy clustering techniques for fuzzy model identification, Elsevier Journal of Fuzzy Sets and Systems 106 (1999) 179–188.
[13] S. Chiu, Fuzzy model identification based on cluster estimation, Journal of Intelligent and Fuzzy Systems 2 (3) (1994) 267–278.
[14] R. Yager, D. Filev, Generation of fuzzy rules by mountain clustering, Journal of Intelligent and Fuzzy Systems 2 (1995) 209–219.
[15] H.J. Truswell, M.-Y. Chow, S. Altug, Heuristic constraints enforcement for training of and knowledge extraction form a fuzzy/nueral architecture—Part I: Foundation, IEEE Transactions on Fuzzy Systems 7 (2) (1999).
[16] W. Sienel, Robust decoupling for active car steering holds for arbitrary dynamic tire characteristics, in: Proceedings of 3rd European Control Conference, Rome, 1995, pp. 744–748.
[17] M. Sugeno, On stability of fuzzy systems expressed by fuzzy rules with singleton consequents, IEEE Transactions on Fuzzy Systems 7 (2) (1999).
[18] J.T. Economou, A. Tsourdos, B.A. White, P.C.K. Luk, Takagi–Sugeno model synthesis of a quasilinear multiwheeled mobile robot, International Journal of Systems Science 34 (14–15) (2003) 805–818.
[19] T.D. Gillespie, Fundamentals of Vehicle Dynamics, Society of Automotive Engineers, Inc., Berlin, 1992, ISBN 1-56091-199-9.